

Phases of ^4He and H_2 adsorbed on doped graphene

M. C. Gordillo^{1,2}

¹*Departamento de Sistemas Físicos, Químicos y Naturales,
Universidad Pablo de Olavide, Carretera de Utrera km 1, E-41013 Sevilla, Spain and*

²*Instituto Carlos I de Física Teórica y Computacional,
Universidad de Granada, E-18071 Granada, Spain*

J. Boronat³

³*Departament de Física, Universitat Politècnica de Catalunya, Campus Nord B4-B5, 08034 Barcelona, Spain*

(Dated: October 20, 2023)

The influence of attractive boron impurities, embedded on a graphene sheet, on the phase diagrams of ^4He and H_2 adsorbed on top was studied using the diffusion Monte Carlo method. The doping of graphene was made by distributing the boron atoms following the same pattern found in an experimentally synthesized substrate. Our results show that while the different incommensurate solid phases of both adsorbates remain largely unchanged after doping, the liquid/gas equations of state are significantly different from the ones on pristine graphene. Doping graphene produces new translationally invariant stable phases for ^4He , depending on the concentration of boron impurities, but makes the H_2 ground state to remain solid. In addition, several new registered phases appear for both adsorbates.

I. INTRODUCTION

First and second layers of ^4He and H_2 adsorbed on graphite have been profusely studied both from the experimental [1–8] and theoretical [9–22] points of view, the main motivation being that both are archetypal two-dimensional (2D) many-body quantum systems. Both species have registered $\sqrt{3} \times \sqrt{3}$ solids as ground states, that change upon further loading into incommensurate lattices before promotion to a second layer. In the limit $T = 0$, those second layers are different for both adsorbates: ^4He forms a 2D liquid that solidifies upon loading, while H_2 always remain solid. Both second layer solids could present supersolidity in a narrow density range [21, 22]. The same is true for molecular hydrogen adsorbed on a second layer of a narrow carbon nanotube. On the other hand, the second layer of ^4He on a nanotube is always a liquid [23].

Reducing the dimensionality of the system has been suggested as a possible way of getting a liquid H_2 phase due to a decreasing in the interaction strength. However, two-dimensional molecular hydrogen has been always shown to be a solid because of the relatively large H_2 - H_2 attractive interaction strength, that makes bulk H_2 solidify at $T > 0$. Nevertheless, its low mass and associated large zero point motion would eventually make H_2 a superfluid if a liquid could be supercooled up to low enough temperatures.

A possibility to frustrate the first layer solid phase would be to consider some kind of defects in the substrate with respect to standard graphene. For instance, one can deposit H_2 on a carbon glass surface [24]. Diffusion Monte Carlo calculations of molecular hydrogen adsorbed on such environment indicate that the registered phase is substituted by a superglass [25] with a small but still finite superfluid fraction. Alternatively, one can think about what would happen on novel substrates such

as graphyne [26] or biphenylene [27] sheets, where some new commensurate phases were found for ^4He but that have not been explored as H_2 adsorbents yet.

With the precedent work in mind, one realizes that an unexplored possible way to get stable liquid H_2 could be to consider its adsorption on a surface with impurities embedded in the substrate. In particular, to load H_2 on a graphene sheet in which part of the carbon atoms have been substituted by another species. In this work, we will use the experimentally synthesized substrate of Ref. 28, that includes boron impurities in a graphene layer. In order to disentangle the effect of the impurity- H_2 interactions from that of their location within the surface, we considered both the substrate of Ref. 28 and another setup that includes a pair of boron impurities located in opposite vertices of a graphene hexagon. We used a pair of impurities instead of a single one due to the particular structure of the boron substrate (see below). Our study was extended to ^4He to compare the influence of the adsorbate-adsorbate interaction in the final results.

II. METHOD

Our method is fully microscopic and starts with the Hamiltonian of the system, written as

$$H = \sum_{i=1}^N \left[-\frac{\hbar^2}{2m} \nabla_i^2 + V_{\text{ext}}(x_i, y_i, z_i) \right] + \sum_{i < j}^N V_{\text{pair}}(r_{ij}), \quad (1)$$

where x_i , y_i , and z_i are the coordinates of the each of the N adsorbate particles with mass m . The potential $V_{\text{ext}}(x_i, y_i, z_i)$ accounts for the interaction between each atom or molecule and all the individual atoms in the rigid graphene-with-impurities layer. Those potentials are of Lennard-Jones (LJ) type, with standard parameters taken from Ref. 29 in the case of He-C, and from

Ref. 30 for the H₂-C interaction. The He-B and H₂-B parameters were deduced using Lorentz's rules in the standard way from the C-B ones found in Ref. 31. Those LJ parameters are $\epsilon_{He-B} = 40.2$ K, $\sigma_{He-B} = 2.87$ Å and $\epsilon_{H_2-B} = 105.5$ K, $\sigma_{H_2-B} = 3.10$ Å, what implies interactions more attractive than for their carbon counterparts. We have checked the robustness of our results by varying those sets of parameters and observing the effects on the phase diagrams. We found that for any reasonable change that keeps the interaction more attractive than for the case of pristine graphene, the phase diagrams for both of ⁴He and H₂ were qualitatively similar to those displayed below.

Finally, in Eq. 1, V_{pair} corresponds to the ⁴He-⁴He and H₂-H₂ potentials. We used the standard Aziz [32] and Silvera and Goldman [33] models, both of them depending only on the distance r_{ij} between particles i and j . This last potential includes the C_9 -dependent term that effectively takes into account three-body effects. We used as a simulation cell one of 51.63×51.12 Å², including 1008- N_i carbon atoms, with N_i the number of boron impurities. As indicated previously, we considered the case for $N_i=2$ and that of a regularly located set of boron atoms. To mimic the experimental compound of Ref. 28, N_i should be 48, i.e., 5% of the total number of atoms in the graphene-like layer.

We solve the many-particle imaginary-time Schrödinger equation using the diffusion Monte Carlo (DMC) method. The DMC stochastic algorithm gives us, within some statistical noise, the exact ground-state of the N -particle system. In order to reduce the variance of the statistical estimations one uses the importance sampling technique. This is done by using a time-independent trial wave function which guides the diffusion process implied by the DMC algorithm. In addition, this trial wave function fixes the phase (solid or liquid) of the ensemble of particles. In the present case, the trial function is written as a product of two terms. The first one is of Jastrow type between the adsorbate particles,

$$\Phi_J(\mathbf{r}_1, \dots, \mathbf{r}_N) = \prod_{i < j}^N \exp \left[-\frac{1}{2} \left(\frac{b}{r_{ij}} \right)^5 \right]. \quad (2)$$

The values of b were the same used in previous works, i.e., 3.07 Å for the ⁴He-⁴He case [17] and 3.195 Å for the H₂-H₂ pair [18]. The second part incorporates the presence of C and B atoms and includes the possibility of localization for the solid phases, properly symmetrized,

$$\begin{aligned} \Phi_s(\mathbf{r}_1, \dots, \mathbf{r}_N) = & \prod_i^N \prod_J^{N_S} \exp \left[-\frac{1}{2} \left(\frac{b_S}{r_{iJ}} \right)^5 \right] \\ & \times \prod_{I=1}^N \left[\sum_{i=1}^N \exp \{ -c[(x_i - x_{\text{site},I})^2 + (y_i - y_{\text{site},I})^2] \} \right] \\ & \times \prod_i^N \Psi(z_i). \end{aligned} \quad (3)$$

In Eq. (3), N_S is the number of atoms in the substrate, either carbon or boron. The parameters b_S were taken from previous calculations on similar all-carbon substrates [17, 18]. r_{iJ} are the distances between a particle i (⁴He or H₂) and an atom J of the substrate. On the other hand, $\Psi(z_i)$ is a one-body function that depends solely on the distance z_i of every particle to the graphite plane [17, 18].

The coordinates $x_{\text{site},I}$ and $y_{\text{site},I}$ are the crystallographic positions that define the different solids (registered or incommensurate) that we are going to consider, and whose number is the same as the number of adsorbate particles in those structures. To obtain the layout of any possible commensurate solids in the 48-impurity substrate, we followed the same procedure as in Ref. 25 and look for local minima for the helium atoms or hydrogen molecules above the graphene-with-boron sheet. To this end, we created a two-dimensional grid of regularly spaced points at a distance z_{site} above the carbon-boron layer and calculated $V_{\text{ext}}(x, y, z_{\text{site}})$ at such locations. z_{site} corresponds to the maximum in the $\Psi(z_i)$ function of Eq. 3. Then, we look for the place on that lattice with the minimum value of V_{ext} and search for any other points with the same value of the external potential located at a distance from the first one of, at least, σ_{He-C} or σ_{H_2-C} , respectively. Any set of such equal-valued potential locations will be the crystallographic sites of a registered phase. Fig. 1 displays as full squares those sites for the lowest-density commensurate solid possible for ⁴He, while Fig. 2 shows the results of an identical procedure for H₂. The different sizes of the ⁴He atom and the H₂ molecule account for the number of potential minima and their different locations.

The incommensurate solids are the standard triangular solids found for those adsorbates on graphene or graphite at higher densities [17, 18]. To avoid mismatch problems between the carbon/boron substrate and the adsorbate monolayers, we followed the procedure carried out in previous simulations including two ⁴He or H₂ layers on graphite [21, 22]: we took the larger piece of a triangular solid of a given density that fits in the 51.63×51.12 Å² cell defined by the substrate and consider it to be at the center of a nine-cell supercell structure created by replicating that adsorbate simulation cell by the vectors that define its length and width. Obviously, we have to do the same with the underlying substrate using the appropriate vectors to replicate the 51.63×51.12 Å² box. Then, for each ⁴He or H₂ in the central cell of the triangular solid, we calculated the adsorbate-adsorbate or adsorbate-adsorbent interactions within a given cutoff distance, irrespectively of the location of the other particle, in the central cell or in one of the images produced by replication. That cutoff for the interactions, taken as half of the smallest side of the adsorbate simulation cell, should be large enough to avoid size effects. This way of dealing with the adsorbate/adsorbent of the simulation cells is completely equivalent to the approximation used in Refs. [11, 12, 14, 16], but it makes possible to

consider simulation cells for adsorbate densities beyond those which fit exactly inside the periodicity of the adsorbent cell.

Finally, the c parameters in Eq. (3) were variationally optimized and found to have similar values to the ones for pure graphene. Importantly, the form of Eq. 3 allows for the those solid phases to be supersolid, since ^4He atoms or H_2 molecules could be involved in exchanges to make them indistinguishable from one another [34]. Obviously, this is also true for translationally invariant phases for which $c = 0$.

To avoid any influence of the initial configurations on the simulations results, we used for the energy averages only the last 10^5 Monte Carlo configurations in a typical $1.2 \cdot 10^5$ steps long simulation run. Each Monte Carlo step considers 300 replicas (walkers) to account for all the possible configurations of the system. The number of particles in each adsorbate simulation cell was fixed by the desired densities. Larger number of walkers or longer simulation runs do not change the final results within our numerical accuracy. To avoid the influence of the correlations between configurations in the same run we calculated all the averages using 10 independent DMC histories, and considered only sets of positions located 100 Monte Carlo steps away. The error bars, when given, correspond to the averages of those 10 histories, not on averages within any single run.

III. RESULTS

A. ^4He

The structure of the substrate corresponds to one of the possibilities experimentally synthesized in Ref. 28, and includes only boron impurities embedded in graphene. Similar compounds in which a C-C pair is substituted by a B-N dimer [35] can be found in the literature, but are not the object of this work. Its impurity distribution is depicted in Figs. 1 and 2. There, the open circles stand for the carbon atoms and the solid ones for the boron impurities. Those are distributed in pairs located in opposite vertices of the hexagons that make up the graphene layer. To try to distinguish between the effect of the impurities themselves from that of their distribution, we performed first simulations including a single pair of impurities in the same hexagon. After that, we considered all 48 boron atoms in the $51.63 \times 51.12 \text{ \AA}^2$ cell shown in those figures.

DMC energies per ^4He atom, as a function of the helium surface density ρ_{He} , for the two-impurity case (full symbols) are displayed in Fig. 3 together with the equivalent results for all-carbon graphene (open symbols). The energies for pure graphene are identical to the ones in Ref. 17, obtained for smaller simulation cells. In all cases, the energy per particle when boron atoms are present is lower than for a substrate with no impurities. This is obviously due to the larger ^4He -B interaction in comparison to the

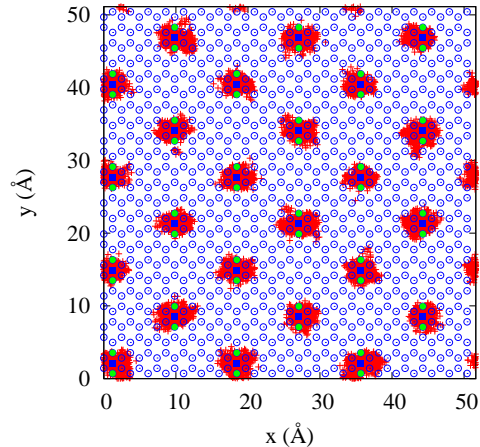


FIG. 1. Structure of the 48-impurities structure used as a substrate in part of the simulations in this work. Open circles, C atoms; solid circles, B atoms. Solid squares, positions corresponding to the 24 locations with the lowest ^4He -substrate potential. Solid smudges are the result of displaying 300 sets of helium coordinates represented as crosses for a registered phase including as many ^4He atoms as potential minima.

^4He -C one. However, we can also see that the difference between those two sets of energies decreases considerably upon helium loading. In fact, the only obvious deviation from the pristine graphene case is produced at low densities and for the translationally invariant phase, whose energy per particle in the infinite dilution limit goes from $-128.26 \pm 0.04 \text{ K}$ for graphene [17] to $-155.4 \pm 0.1 \text{ K}$ for the two-impurity case. The latter result is lower than the corresponding to a registered $\sqrt{3} \times \sqrt{3}$ solid on the same substrate, $-129.69 \pm 0.02 \text{ K}$. This implies that that commensurate structure is not longer the ground state of the helium monolayer. For comparison, the energy per particle of the same $\sqrt{3} \times \sqrt{3}$ arrangement in graphene is $-129.282 \pm 0.007 \text{ K}$ [17].

To obtain the stability limits of the new phase diagram we need to perform double-tangent Maxwell constructions between the different phases. To do so, we have to display the energy per particle versus the inverse of the helium density (or the surface per particle), in the way it is done in Fig. 4. In this analysis, we exclude densities $\rho_{\text{He}} < 3.8 \cdot 10^{-3} \text{ \AA}^{-2}$ because in this regime all He atoms form clusters around the attractive impurities, i.e., do not form an extended phase. The Maxwell anal-

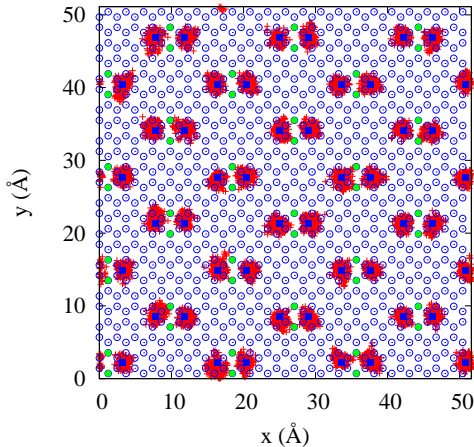


FIG. 2. Same as in Fig. 1, but for the lowest density registered H_2 phase. We have 48 H_2 -substrate potential minima, represented by solid squares. As before, solid smudges are the result of displaying 300 sets of hydrogen coordinates represented as crosses.

ysis shows a translationally invariant phase for densities $0.042 < \rho_{\text{He}} < 0.053 \text{ \AA}^{-2}$. After that, we have a first order phase transition to a standard $\sqrt{3} \times \sqrt{3}$ registered solid with density $\rho_{\text{He}} = 0.0636 \text{ \AA}^{-2}$. That phase will be in equilibrium with an incommensurate arrangement of $\rho_{\text{He}} > 0.070 \text{ \AA}^{-2}$ with energy per particle of $-128.59 \pm 0.01 \text{ K}$ stable, in principle, up to the second layer promotion. This is to be compared with a lower limit for the incommensurate structure for graphene of $\rho_{\text{He}} = 0.080 \text{ \AA}^{-2}$ with energy per particle of $-126.6 \pm 0.2 \text{ K}$ [17].

Fig. 5 displays the energy results for the substrate including 48 boron atoms, already depicted in Fig. 1. There, we can see that the energy per particle is lower than the one for graphene and lower than the one for the two-impurity case. In Fig. 5, the open circles correspond to commensurate structures, while the solid ones show the results for the translationally invariant phase (circles) and the incommensurate solid (squares).

The registered phase with the lowest density, represented by the set of smudges in Fig. 1, is the ground state for this substrate, with a density of 0.009 \AA^{-2} (24 ^4He atoms in the simulation cell) and an energy per particle of $-155.7 \pm 0.1 \text{ K}$, slightly lower than the one corresponding to the infinite dilution limit, $-155.4 \pm 0.1 \text{ K}$ and equal to the value for the two-impurities substrate. This

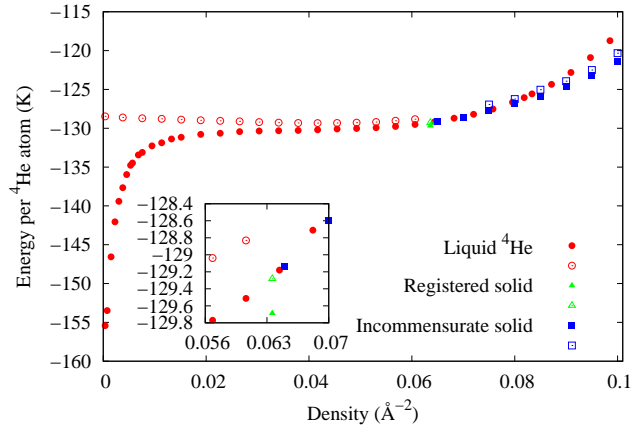


FIG. 3. Energy per ^4He atom as a function of helium density for pristine graphene (open symbols) and for graphene including only two boron impurities (solid symbols). The inset shows the same data around the density corresponding to the commensurate solids. The error bars are of the size of the symbols and not shown for simplicity.

small difference could be assigned to the residual ^4He - ^4He interaction energy of particles located $\sim 10 \text{ \AA}$ apart. The other commensurate structure corresponds to the $\sqrt{3} \times \sqrt{3}$ solid and, as it can be seen both in Fig. 5 and 6, its energy per particle is slightly larger ($-143.19 \pm 0.02 \text{ K}$), than the corresponding to a translationally invariant structure ($-143.24 \pm 0.02 \text{ K}$, from the least-squares fitting line in Fig. 6). This means that is unstable (if barely) with respect to that last arrangement. No other stable registered phases were found.

Using Figs. 5 and 6, we can get the stability limits for the different phases on the 48-impurity substrate by means of double-tangent construction lines, an example of which is given in Fig. 6. The commensurate 24-atom registered solid is in equilibrium with a translationally invariant structure stable in the $0.038 < \rho_{\text{He}} < 0.072 \text{ \AA}^{-2}$ range. The energies per particle for those densities are $-150.6 \pm 0.1 \text{ K}$ and $-141.7 \pm 0.1 \text{ K}$, respectively. Upon further loading, there is a first order transition to an incommensurate triangular solid of density $\rho_{\text{He}} = 0.085 \text{ \AA}^{-2}$ and energy per ^4He atom of $-138.9 \pm 0.1 \text{ K}$. This means that we have reentrant behaviour from a very low-density commensurate solid created by the presence of the attractive boron impurities to a liquid at intermediate densities.

B. H_2

Fig. 7 is the counterpart of Fig. 3 for the case of H_2 . We compare the energies for H_2 on pure graphene and with graphene doped with two B impurities. As before, the energy per H_2 molecule for all values of the hydrogen density, ρ_{H_2} , is smaller than for pristine graphene

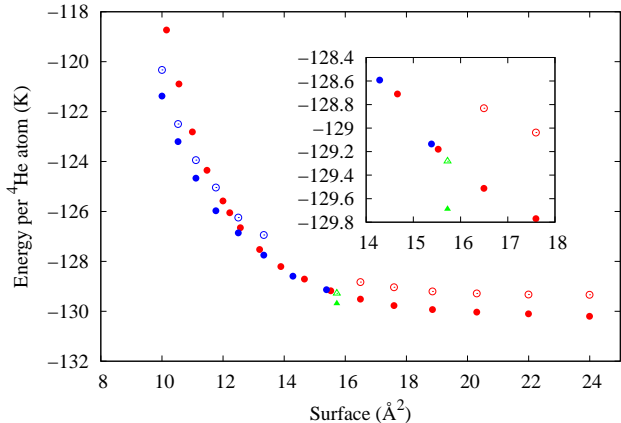


FIG. 4. Same as in the previous figure but displaying the energy as a function of the surface per ${}^4\text{He}$ atom. The symbols have the same meaning as in Fig. 3. Again, we show an inset around the surface per atom corresponding to the registered $\sqrt{3} \times \sqrt{3}$ phase for both substrates.

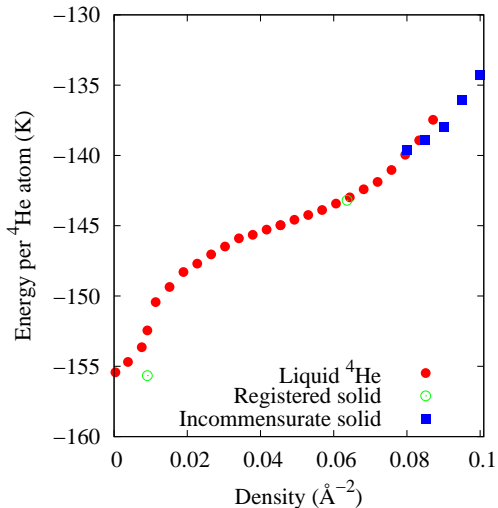


FIG. 5. Energy per ${}^4\text{He}$ atom as a function of helium density for graphene including 48 boron impurities. The open circles correspond to two different registered phases. The solid circles are data for a translationally invariant structure, while the solid squares are the energy per atom of an incommensurate solid. and open. The error bars are of the size of the symbols and not shown for simplicity.

due to the larger $\text{H}_2\text{-B}$ attraction in comparison to the $\text{H}_2\text{-C}$ one. Again, the infinite dilution limit when boron impurities are present is lower (-515.6 ± 0.1 K) than for the all-carbon substrate (-431.79 ± 0.06 K) [18] and for the $\sqrt{3} \times \sqrt{3}$ commensurate phase, whose energy (-463.6 ± 0.02 K) is displayed in Fig. 7 as a solid triangle. The open triangle in the same figure corresponds to the

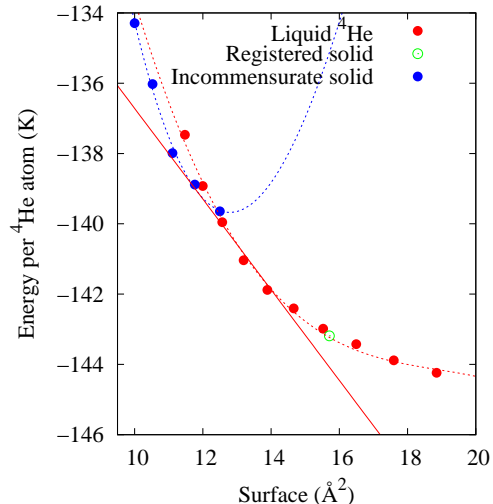


FIG. 6. Same as in the previous figure but displaying the energy as a function of the surface per ${}^4\text{He}$ atom. Dotted lines are third order least-squares polynomial fits to the simulation data displayed as solid symbols. Full line, Maxwell construction between a liquid of density 0.072 \AA^{-2} and an incommensurate solid phase of 0.085 \AA^{-2} .

same structure in graphene (-461.12 ± 0.01 K [18]). An analysis of the hydrogen configurations in the DMC runs indicates that for densities $\rho_{\text{H}_2} < 0.0015 \text{ \AA}^{-2}$ there is not an extended phase but a cluster of 3-5 molecules located close to the two-boron impurities. The $\sqrt{3} \times \sqrt{3}$ registered structure is in equilibrium with an incommensurate triangular solid of density $\rho_{\text{H}_2} = 0.075 \text{ \AA}^{-2}$ and energy per particle -455.84 ± 0.02 K. That density is comparable to the one for the pure substrate ($\rho_{\text{H}_2} = 0.077 \text{ \AA}^{-2}$ [18]), while the energy per molecule in graphene is a little bit larger (-452.08 ± 0.01 K [18]).

The energy per particle as a function of ρ_{H_2} for the 48-impurity substrate is displayed in Fig. 8. As before, the open circles stand for different registered phases. The set of crystallographic positions that define those commensurate structures were obtained by the potential minima searching algorithm described above. The only difference is that instead of having only one of such structures, we have three of them, displayed in Figs. 2, 9 and 10. The remaining registered phase of density 0.0636 \AA^{-2} is the standard $\sqrt{3} \times \sqrt{3}$ structure. The different energies per

TABLE I. Densities and energies per H_2 molecule of the stable registered phases for the 48-impurities substrate.

Number of H_2 molecules	ρ_{H_2} (\AA^{-2})	Energy (K)
48	0.018	-517.4 ± 0.1
96	0.036	-509.8 ± 0.1
168 ($\sqrt{3} \times \sqrt{3}$)	0.0636	-504.9 ± 0.1
192	0.073	-497.5 ± 0.1

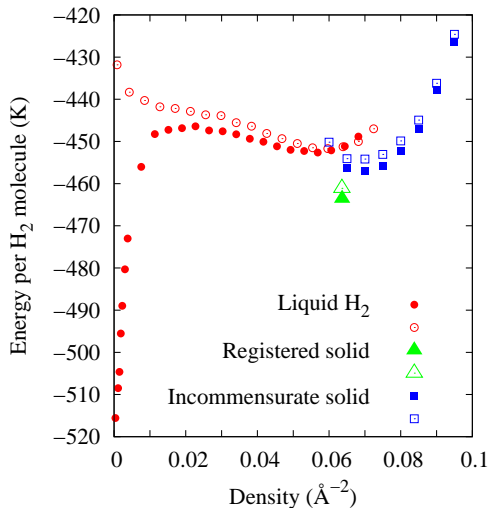


FIG. 7. Energy per H₂ molecule as a function of hydrogen density for pure graphene (open symbols) and for two-boron impurity graphene (solid symbols). The error bars are of the size of the symbols.

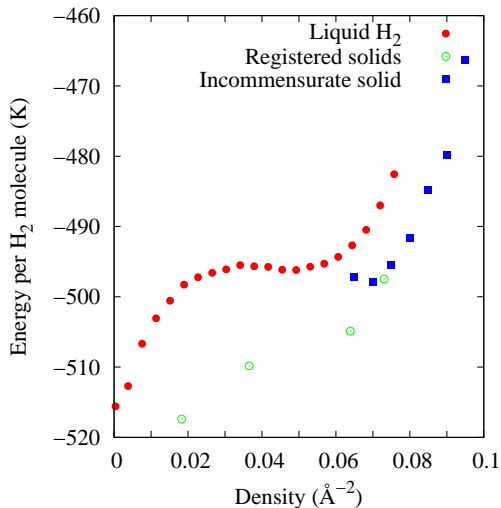


FIG. 8. Same as in the previous figure but for a 48-impurities substrate. Open circles, registered phases; solid circles, translationally invariant structure; solid squares, incommensurate triangular solid.

particle and densities for those arrangements are listed in Table I.

As it is shown in Fig. 8, all the registered phases have energies lower than the ones for translationally invariant distributions with the same hydrogen density. In particular, the most stable phase has an energy per H₂ molecule 1.8 K lower than the corresponding to the infinite dilution limit. That arrangement is now the ground state

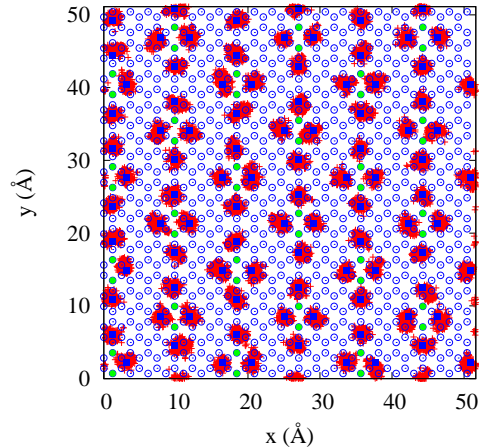


FIG. 9. Same as in Fig. 2 but for a structure with 96 potential minima. The symbols have the same meaning as in that figure.

and we should see upon loading a series of first order phase transitions between all the solids in Table I. From the last of those distributions, we can draw a Maxwell construction with a common tangent to an incommensurate solid with $\rho_{\text{H}_2} = 0.075 \text{ \AA}^{-2}$ and energy per molecule of -495.5 ± 0.4 K. That would be the stable structure up to a second layer promotion.

IV. DISCUSSION

Examining the phase diagrams of both adsorbates with the introduction of impurities, we can see that the larger changes with respect to what happens in pristine graphite happen for translationally-invariant phases at very low densities. In those cases, the analysis of the DMC configurations indicates that they are made up of small clusters of ⁴He or H₂ close to a set of two boron impurities. This means that there is not a stable extended phase of the type of a conventional liquid or gas. In addition, the energy per particle of those small clusters decreases drastically with respect to the infinite dilution limit of an all-carbon substrate. Since the influence of the boron impurities on the ⁴He/H₂ behavior decreases when the density increases, the overall effect is of a drastic change in the equation of state of those translationally-invariant phases. That can be seen clearly in Figs. 3, 5, 7 and

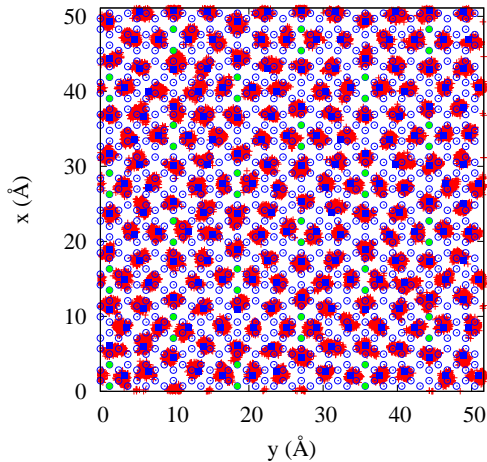


FIG. 10. Same as in Figs. 2 and 9 but for a registered solid with 192 crystallographic positions in the simulation cell.

8. In any case, those isolated cluster arrangements are only stable when the number of adsorbed particles and boron impurities is very small. When we have enough atoms or molecules to form clusters close to neighboring pairs of boron atoms, as in the case in which we have 48 boron impurities, a commensurate low density ground state is produced whose nature depends on the details of the adsorbate-substrate potential.

Beyond those small densities, we can see that the variations in the ^4He phase diagram depend basically on the number of boron atoms in the substrate. For instance, in the two-impurities case, the upper density limit is basically unchanged with respect to that of pristine graphene, with a stable $\sqrt{3} \times \sqrt{3}$ phase that transforms upon loading into a incommensurate triangular solid. On the other hand, when we have 48 boron impurities, the decrease of the energy per ^4He atom in the translationally invariant phase, make it (barely) more stable than a $\sqrt{3} \times \sqrt{3}$ solid of the same density. However, the difference is small and could depend on the particular distribution of the boron atoms. In any case, we have two phases very close in energy, as in pure graphene [17]. When the helium density increases, we end up with the same type of incommensurate solid structures as in an all-carbon substrate.

For the same 48-boron substrate, the energy per particle of the H_2 translationally invariant phase is always larger than the corresponding to the different registered phases. This means that that arrangement is unstable, and the only difference with respect to the graphene case will be the appearance of other solids, i.e., a liquid H_2 phase cannot be achieved by introducing attractive impurities in the substrate. An interesting question is the possibility that any of those registered solids could be a supersolid. The trial wave function (3) allows for the possibility of exchanges between particles, a necessary ingredient to have supersolids. However, we have verified that none of the commensurate solids show a nonzero value for the superfluid density. The same null result is obtained for the $\sqrt{3} \times \sqrt{3}$ phase in the two-impurity helium case. This means that the introduction of impurities destroys the small superfluid fraction found for pristine graphene [34].

From all the results above it is clear that, in order to get superfluid/supersolid behavior in H_2 it is not useful to use a substrate with a regularly disposed set of attractive impurities. This produces only new registered phases. We will have to think of a situation in which no commensurate phases are possible, and the equation of state of the translationally invariant structure can be changed enough to produce a supersolid. Taking all of that in mind, the only successful substrate up to now is the carbon glass already considered in Ref. [25], whose irregular structure is able to stabilize a superglass, but not a superfluid.

ACKNOWLEDGMENTS

We acknowledge financial support from Ministerio de Ciencia e Innovación MCIN/AEI/10.13039/501100011033 (Spain) under Grants No. PID2020-113565GB-C22 and No. PID2020-113565GB-C21 and from Junta de Andalucía group PAIDI-205. M.C.G. acknowledges funding from European regional development fund (FEDER) and Junta de Andalucía Economy, Knowledge, Business and University Consejería under their specific goal 1.2.3 of the FEDER program Andalucía 2014-2020 “Promotion and generation of frontier knowledge and knowledge aimed at the challenges of society, development of emerging technologies.” under Grant No. UPO-1380159, FEDER-financed percentage 80% and J.B. from AGAUR-Generalitat de Catalunya Grant No. 2021-SGR-01411. We also acknowledge the use of the C3UPO computer facilities at the Universidad Pablo de Olavide.

[1] P. A. Crowell and J. D. Reppy, Reentrant superfluidity in ^4He films adsorbed on graphite,

Phys. Rev. Lett. **70**, 3291 (1993).

- [2] P. A. Crowell and J. D. Reppy, Superfluidity and film structure in ^4He adsorbed on graphite, *Phys. Rev. B* **53**, 2701 (1996).
- [3] D. S. Greywall and P. A. Busch, Heat capacity of fluid monolayers of ^4He , *Phys. Rev. Lett.* **67**, 3535 (1991).
- [4] D. S. Greywall, Heat capacity and the commensurate-incommensurate transition of ^4He adsorbed on graphite, *Phys. Rev. B* **47**, 309 (1993).
- [5] O. E. Vilches, Search for low temperature liquid H_2 in 2-D films, *J. Low Temp. Phys.* **89**, 267 (1992).
- [6] H. Wiechert, in *Excitations in Two-Dimensional and Three-Dimensional Quantum Fluid*, edited by A. Wyatt and H. Lauter (Plenum, New York, 1991).
- [7] J. Nyeki, A. Phillis, A. Ho, D. Lee, P. Coleman, J. Parpia and B. Cowan, and J. Saunders, Intertwined superfluid and density wave order in two-dimensional ^4He , *Nat. Phys.* **13**, 455 (2017).
- [8] S. Nakamura, K. Matsui, T. Matsui, and H. Fukuyama, Possible quantum liquid crystal phases of helium monolayers, *Phys. Rev. B* **94**, 180501(R) (2016).
- [9] P. A. Whitlock, G. V. Chester, and B. Krishnamachari, Monte carlo simulation of a helium film on graphite, *Phys. Rev. B* **58**, 8704 (1998).
- [10] P. Corboz, M. Boninsegni, L. Pollet, and M. Troyer, Phase diagram of ^4He adsorbed on graphite, *Phys. Rev. B* **78**, 245414 (2008).
- [11] M. Pierce and E. Manousakis, Phase diagram of second layer of ^4He adsorbed on graphite, *Phys. Rev. Lett.* **81**, 156 (1998).
- [12] M. Pierce and E. Manousakis, Path-integral monte carlo simulation of the second layer of ^4He adsorbed on graphite, *Phys. Rev. B* **59**, 3802 (1999).
- [13] M. E. Pierce and E. Manousakis, Role of substrate corrugation in helium monolayer solidification, *Phys. Rev. B* **62**, 5228 (2000).
- [14] M. E. Pierce and E. Manousakis, Monolayer solid ^4He clusters on graphite, *Phys. Rev. Lett.* **83**, 5314 (1999).
- [15] K. Nho and E. Manousakis, Submonolayer molecular hydrogen on graphite: A path-integral monte carlo study, *Phys. Rev. B* **65**, 115409 (2002).
- [16] K. Nho and E. Manousakis, Commensurate-incommensurate transitions in quantum films: Submonolayer molecular hydrogen on graphite, *Phys. Rev. B* **67**, 195411 (2003).
- [17] M. C. Gordillo and J. Boronat, ^4He on a single graphene sheet, *Phys. Rev. Lett.* **102**, 085303 (2009).
- [18] M. C. Gordillo and J. Boronat, Phase diagram of H_2 adsorbed on graphene, *Phys. Rev. B* **81**, 155435 (2010).
- [19] M. C. Gordillo and J. Boronat, Second layer of H_2 and D_2 adsorbed on graphene, *Phys. Rev. B* **87**, 165403 (2013).
- [20] M. C. Gordillo and J. Boronat, Zero-temperature phase diagram of the second layer of ^4He adsorbed on graphene, *Phys. Rev. B* **85**, 195457 (2012).
- [21] M. C. Gordillo and J. Boronat, Superfluid and Super-solid Phases of ^4He on the Second Layer of Graphite, *Phys. Rev. Lett.* **124**, 205301 (2020).
- [22] M. C. Gordillo and J. Boronat, Supersolidity in the second layer of para- H_2 adsorbed on graphite, *Phys. Rev. B* **105**, 094501 (2022).
- [23] M. C. Gordillo, R. Rodríguez-García, and J. Boronat, Phases of ^4He and h_2 adsorbed on a single carbon nanotube, *Phys. Rev. B* **107**, 174518 (2023).
- [24] C. Toh, H. Zhang, J. Lin, A. S. Mayorov, Y. Wang, C. M. Orofeo, D. B. Ferry, H. Andersen, N. Kakenov, Z. Guo, I. H. Abidi, H. Sims, K. Suenaga, S. T. Pantelides, and B. Ozyilmaz, Synthesis and properties of free-standing monolayer amorphous carbon, *Nature (London)* **577**, 199 (2020).
- [25] M. C. Gordillo and J. Boronat, H_2 super-glass on an amorphous carbon substrate, *Phys. Rev. B* **107**, L060505 (2023).
- [26] J. Ahn, M. You, G. Lee, T. Volkoff, and Y. Kwon, Symmetry-changing commensurate-incommensurate solid transition in the ^4He monolayer on 6,6,12-graphyne, *Phys. Rev. B* **99**, 024113 (2019).
- [27] J. Ahn and Y. Kwon, Vacancy-induced supersolidity of the second ^4He layer on a biphenylene carbon sheet, *Phys. Rev. B* **107**, 094510 (2023).
- [28] S. Kawai, S. Saito, S. Osumi, Y. Yamaguchi, A. S. Foster and P. Spijker, and E. Meyer, Atomically controlled substitutional boron-doping of graphene nanoribbons, *Nat. Commun.* **6**, 8098 (2015).
- [29] W. E. Carlos and M. W. Cole, Interaction between a He atom and a graphite surface, *Surf. Sci.* **91**, 339 (1980).
- [30] G. Stan and M. W. Cole, Hydrogen adsorption in nanotubes, *J. Low Temp. Phys.* **110**, 539 (1998).
- [31] Y. Pan, L. Li, X. Yuan J. Guo, and P. Yang, Effects of defects on heat conduction of graphene/hexagonal boron nitride heterointerface, *Phys. Lett. A.* **4**, 126774 (2020).
- [32] R. Aziz, F.R.W McCourt, and C. K. Wong, A new determination of the ground state interatomic potential for He_2 , *Mol. Phys.* **61**, 1487 (1987).
- [33] I. F. Silvera and V. V. Goldman, The isotropic intermolecular potential for H_2 and D_2 in the solid and gas phases, *J. Chem. Phys.* **69**, 4209 (1978).
- [34] M. C. Gordillo, C. Cazorla, and J. Boronat, Supersolidity in quantum films adsorbed on graphene and graphite, *Phys. Rev. B* **83**, 121406(R) (2011).
- [35] R. Pawlak, K. N. Anindya, T. Shimizu, J.C. Liu, T. Sakamaki, R. Shang, A. Rochefort and E. Nakamura, and E. Meyer, Atomically precise incorporation of bn-doped rubicene into graphene nanoribbons, *J. Phys. Chem. C* **126**, 19726 (2022).